Title:	Morphological Transformations During Activation and Reaction of an Iron Fischer-Tropsch Catalyst
PI (Authors):	Nancy B. Jackson[1], Steven Kohler[1], Mark Harrington[1], Allen Sault[1], Abhaya K. Datye[2], Mehul D. Shroff[2], and Dinesh S. Kalakkad[2]
Institution/Organization:	[1]Sandia National Laboratories, Albuquerque, NM 87185 [2]University of New Mexico, Albuquerque, NM 87131
Contract Number:	DE-AC04-94AL85000
Period of Performance:	10/1/94-9/30/95

Objective

The purpose of this project is to support the development of slurry-phase bubble column processes being studied at the La Porte Alternative Fuel Development Unit. This paper describes the aspects of Sandia's recent work regarding the advancement and understanding of the iron catalyst used in the slurry phase process. A number of techniques were used to understand the chemical and physical effects of pretreatment and reaction on the attrition and carbon deposition characteristics of iron catalysts. Unless otherwise stated, the data discussed below was derived from experiments carried out on the catalyst chosen for the summer 1994 Fischer-Tropsch run at LaPorte, UCI 1185-78-370, (an L 3950 type) that is 88% Fe_2O_3, 11% CuO, and 0.052% K_2O.

Experimental

The catalyst used in this study was precipitated from an iron sulfate precursor and spray - dried. The CO used was Matheson research purity 99.99% and was further purified to remove carbonyls by passing it through a column containing glass beads heated to 600 K, an ascarite column and a 7 μm Swagelok particle filter. H_2 and He were UHP 99.999% Alphagaz and Argyle, respectively. The He was further purified by passing it through an AllTech Oxy-Trap. The O_2 used in passivation was Big 3 UHP 99.993%. The GC He was Argyle UHP 99.999%. The reactor was a differential fixed bed reactor consisting of a quartz glass U-tube with a bulb in which a known weight of catalyst (approximately 1 g.) was placed over a quartz wool plug. The reactor was enclosed by an electrically heated Griffin-Type Series-O heating mantle (750 W) and the catalyst temperature was monitored and controlled by a thermocouple connected to a PID controller which maintained the temperature to within 2 K of the set temperature. The gas flow rates were set and controlled by Tylan FC-260 mass flow controllers calibrated for the specific gases used and were maintained to within 1 sccm for helium and 0.1 sccm for the other gases.

In all the studies, approximately 1 gram of the as-received catalyst was loaded into a tubular, fixed-bed reactor. Different batches were activated under different activation conditions. These were:

a. CO (containing 3% Ar as internal standard) - 20.6 sccm, 543 K, 2 h.
b. H_2:CO - 3.5:5.2 sccm, 543 K, 2h.
c. H_2:CO - 3.5:5.2 sccm (FTS reaction mixture with $H_2/CO = 0.7$), 523 K, 2 h.
d. H_2 - 20 sccm, 543 K, 100 h
e. H_2 - 20 sccm, 723 K, 15 h

After activation, reactions were carried out over the catalyst samples in the same reactor tube at 523 K with $H_2/CO = 0.7$ and a total gas flow rate of 8.7 sccm (H_2:CO/Ar=3.5:5.2 sccm) at a pressure of 630 Torr (normal atmospheric pressure in Albuquerque). Samples were collected at different points along the experiment including the just-activated sample, activated and used for FT reaction for 10 hours, and activated sample used for FT reaction for 45 hours. Before switching the flowing gases from the activation mixture to the reaction mixture, the reactor was cooled to room temperature and extensively purged with helium. In the case of the syngas activation, the first two hours of the reaction run were considered the activation step.

The samples were removed from the reactor after careful and highly controlled passivation. This involved cooling the sample to room temperature, purging with He and exposing to small amounts of O_2 in a stream of flowing He until a final content of 20% was reached. The completion of the passivation process was marked by the occurrence of a small exotherm (typically 2-3 K) in the catalyst bed and the subsequent return to room temperature. The sample was then removed and stored in a glass vial for further characterization tests. To assess the efficacy of the passivation step, we examined a catalyst that was reduced in H_2 at 673K and was transformed into metallic Fe and subsequently passivated. TEM images showed a thin film of magnetite after air exposure, which was no more than 1-2 nm thick. The passivation-grown magnetite film was crystalline and therefore easy to distinguish from the amorphous carbon films that resulted from use of the catalyst in the FT environment.

The product gases were analyzed in a Varian 3400 Gas Chromatograph (GC) and the peak areas were integrated by a Varian 4270 integrator. Analyses were done with a Thermal Conductivity Detector (TCD) with He as a reference gas for the detector. The CO feed stream had 3% Ar as an internal standard so that the conversion of CO could be directly measured. The column used was a 80/100 0.125" x 15' stainless steel column with Supelco Carboxen^{TM} 1000 packing.

The catalyst microstructures were studied by both scanning and transmission electron microscopy using a Hitachi S-800 SEM, JEOL JEM 2000FX TEM (3.0 Å point resolution) and a JEM 2010 TEM (1.9 Å point resolution). For the TEM, the sample was mounted on a copper grid with holey carbon. The grids were dipped into the sample and the excess sample was shaken off. No solvents were used at any stage of the process.

Surface areas were measured using the B.E.T. method using a Micromeritics ASAP 2000 instrument. Carbon content was measured with a Perkin-Elmer 2400 CHN Elemental Analyzer to quantify carbon content of the catalyst samples. This involved oxidizing the samples at 1000 K and measuring the amount of CO_2 formed. Powder X-ray diffraction (XRD) patterns obtained done on all the samples in order to estimate the relative amounts of phases present. Since no internal standard was used in these experiments, the peak area serves only as a qualitative measure of the amount of each phase present. However, determination of peak areas permits a better estimate of the carbide peak since it overlaps with one of the magnetite peaks.

All X-ray photoelectron spectroscopy (XPS) and Auger electron spectroscopy (AES) experiments were performed in an ultra-high vacuum (UHV) chamber coupled to an atmospheric pressure reaction cell. This apparatus is identical to one described elsewhere except that facilities for X-ray photoelectron spectroscopy (XPS) and ion scattering spectroscopy (ISS) have been added. All XPS and AES results were obtained from samples treated in situ in the reaction cell and transferred into UHV without exposure to air. Detailed treatment procedures are described in reference AES was performed using a Perkin-Elmer Model 15-155 cylindrical mirror analyzer, with excitation of

the Auger process provided by a 3 keV, 4 μA, 100 μm diameter electron beam generated by a coaxial electron gun mounted within the analyzer. Details of data collection and manipulation are provided elsewhere[1]. XPS was performed with a VG Microtech CLAM2 hemispherical analyzer operated at a pass energy of 50 eV and a slit width of 4 mm. A 600W Al Kα X-ray source oriented 50° away from the analyzer lens axis provided primary excitation. The XPS energy scale was calibrated by measuring the positions of the Cu 2p3/2 (932.7 eV) and Cu 3p (75.1 eV) peaks from the copper sample holder[2]. Both XPS and AES data are plotted by drawing straight lines between individual data points without any smoothing or curve fitting. XPS peak assignments are based on comparison of peak shapes and binding energies with accepted literature values for metallic iron and iron oxides, as summarized by Kuivila, et al.[3] while AES lineshape analysis is based on reference[4].

Results

The rate of CH_4 formation is plotted in Figure 1 and is used as an indicator of the FTS activity of these samples. It is seen that activation in CO produces the most active catalyst. The activity of the two samples activated in synthesis gas approach one another over time, however the catalyst activated at 543 K is active more quickly than the catalyst activated at 523 K. What is not indicated on Figure 1, are the CH_4 formation rates for the H_2 treated samples. Neither H_2-treated sample demonstrated any Fischer-Tropsch activity.. The sample reduced in H_2 at 543 K produced some CO_2 upon reaction with synthesis gas, but the sample reduced in H_2 at 723 K did not even produce CO_2. We have not quantified any hydrocarbons other than CH_4 since our GC system was not set up for this purpose. We were able to detect C_2 and C_3 in small amounts, but the peaks were extremely broad under our experimental conditions. We also detected hydrocarbon oils when the catalyst was removed after reaction. These oils accumulated at the bottom of the quartz U-tube reactor, but were not quantified. The CH_4 formation rate is therefore the only indicator of FT activity of this catalyst.

CHN Analysis

Table 1 shows the results of CHN analysis used to determine the weight percent carbon as a function of activation and reactions. (The calculated carbon content for the various carbide phases are 6.7% in Fe_3C, 7.9% in χ-$Fe_{2.5}C$, 8.9% in ε'-$Fe_{2.2}C$, and 9.7% in ε-Fe_2C.)

Table 1. Carbon Content (wt%) as a function of activation and reaction. (Rxn T=523 K)

TYPE	ACTIVATION	SHORT REACTION	LONG REACTION
CO/543 K	3.1	6.85	10.6
CO&H_2/523 K	0.2	1.6	5.1
CO&H_2/543 K	0.6	2.3	5.3
H_2/543 K	0	n/a	3.6

XRD Analysis

X - ray powder diffraction patterns of the CO - activated sample after activation, and after 10 and 45 hours of FT synthesis show that it is predominantly magnetite with a small amount of carbide after the activation step. See Table 2. It gradually transforms almost completely into carbide after exposure to syngas at 523 K for 45 hours. The prominent magnetite peaks are seen at the following 2θ values: 30°, 35.5°, 43°, 53.5°, 57°, and 62.7°. The carbide peak at around 43° was found to overlap with the magnetite peak at the same 2θ value. Since we did not use an internal standard, direct quantification of the amounts of various phases present was not possible. We have therefore used the peak area for most intense reflection for each phase as a qualitative measure of

the amount of that phase. For the carbide phase, this was only possible after the area of the magnetite peak at that same 2θ value (scaled with respect to the most intense reflection) was first subtracted. The samples that were activated in synthesis gas were also initially found to be predominately magnetite and after reaction had increasing amounts of carbide present.

Table 2. Analysis of XRD Patterns

Treatment	Ratio of XRD peak at 35.5° to that at 43°	Carbide X 100 (Carbide+Magnetite)
CO activation 543K 2 h	2.12	36.0
activation + 10 h CO/H_2	0.99	70.1
activation + 45 h CO/H_2	0.00	100.0
CO/H_2 activation 523 K 2 h	3.33	0.00
activation + 10 h CO/H_2	2.43	26.8
activation + 45 h CO/H_2	1.21	63.4

BET Surface Area

The surface areas were determined by a multi-point BET isotherm and are listed in Table 3. The as-received sample had a BET surface area of 27 m^2/g. Activation of the sample causes a significant increase in surface area for the CO activated sample. With increasing times on stream, the BET surface areas of all three samples tend to converge and are only marginally different from the initial surface area. While the surface areas, by themselves, do not provide any indication for the changes in catalyst morphology, the electron micrographs reveal major structural rearrangement to be occurring as the sample is activated and used for F-T synthesis.

Table 3. BET surface area (m^2/g)

TYPE	ACTIVATION	SHORT RXN.	LONG RXN.
H_2/543 K	5		
CO/543 K	44.22	33.59	23.17
FTS/523 K	31.76	28.25	24.35

Surface Analysis

For the freshly calcined sample, XPS detects Fe_2O_3 as the sole iron phase present. In addition, copper, potassium, and small amounts of magnesium are observed on the catalyst surface. Since we are unaware of any intentional addition of Mg to the catalyst, it must be assumed that the Mg arises from minor impurities introduced during catalyst synthesis. XPS (Fig. 2) and AES (Fig. 3) spectra were also taken after each activation treatment. After both CO and syngas activation treatments, a single Fe $2p_{3/2}$ XPS peak is observed at a binding energy of 710.8 eV. The position of this peak, coupled with the absence of any shakeup features between 715 and 720 eV, unambiguously identifies magnetite as the primary phase detected in both cases. No evidence is seen for metallic iron or iron carbide phases, which would appear near 707 eV, or carbidic carbon, which would appear at ~283 eV. While the XPS result for syngas activation is in complete agreement with XRD and TEM, the absence of any carbide following CO activation is surprising given that XRD and TEM detect carbide. Based on past measurements of mixed iron carbide/oxide phases with this instrument, carbide levels as low as 4-5% should be detectable, leading to the conclusion that no more than 2-3% of the total surface iron detected is present as carbide following CO activation at 543K for 2 h. AES supports the XPS analysis, showing a two peak structure in the Fe(MVV) region between 40 and 55 eV, characteristic of iron oxides[5]. Furthermore, the O(511 eV)/Fe(703 eV) ratios are lower than expected for Fe_2O_3, and the relative

sizes of the three Fe(LMM) peaks at 598, 651, and 703 eV are intermediate between those of Fe_2O_3 and metallic iron[5]. Taken together, this information supports assignment of the Auger spectra for the CO and syngas activated samples to magnetite.

In order to assess the ability of XPS to detect iron carbide in these catalysts, a sample of the catalyst after hydrogen activation and FT synthesis for 45 h was analyzed by XPS. Even though XRD (Table 2) and TEM (see below) show that more than half the iron in this sample is carbided, XPS detects no carbide whatsoever. TEM shows that the carbide particles are covered by 3-4 nm amorphous carbon films, which undoubtedly severely attenuate the Fe 2p carbide signal and prevent its detection in the presence of magnetite. In support of this argument are the results of a depth profiling experiment in which the sample was bombarded with 5 kV Ar^+ ions at a current density of 1 $\mu A/cm^2$ for 1 h. Following this treatment, shoulders appeared in both the Fe 2p and C 1s regions at energies of 707 eV and 283 eV, respectively, much as observed by Reymond et al.[6] This result is a clear indication of the presence of carbide buried beneath a second phase. We will return to this point later in the discussion section.
XPS and AES detect small amounts of carbon on both the CO and syngas activated samples, with C 1s binding energies and C(272 eV) Auger peak shapes characteristic of graphitic carbon[5]. While Fig. 3 shows a larger carbon signal for the CO activated sample than the syngas activated sample, this result was not reproducible, possibly due to uncertainties in sample temperature measurements discussed in reference 4. It is clear, however, that carbon levels increase with activation time for both treatments. Although no carbidic carbon is seen by either XPS or AES, it is probable that graphitic overlayers on the carbide phase severely attenuate the carbide signals, as described above for attenuation of the Fe 2p carbide signal, and thereby prevent their detection.

XPS and AES of the hydrogen activated sample show nearly complete reduction to metallic iron. The Fe $2p_{3/2}$ binding energy of 707 eV, and the single Fe(MVV) Auger peak at 47 eV are clear indicators of metallic iron. A small shoulder at ~710 eV on the Fe $2p_{3/2}$ peak and subtle differences between the Fe(MVV) lineshape of the activated sample and that of metallic iron[4] indicate the presence of some residual oxide. Note that the presence of a relatively large O(511 eV) peak cannot be taken as a direct indicator of iron oxidation since a fraction of the oxygen is associated with potassium[4]. Detailed Fe(MVV) lineshape analysis[4] suggests that 35 to 45% of the O(511 eV) signal is due to iron oxides while the remainder is associated with potassium.

In addition to demonstrating iron reduction during hydrogen activation, the XPS and AES results also show the appearance of large amounts of sulfur on the surface and growth of the potassium signal relative to iron. The growth of the potassium signal is attributed to the loss of surface area during reduction, which increases the potassium coverage. The appearance of sulfur is attributed to migration of sulfate impurities in the catalyst to the catalyst surface. Rough quantitative analysis shows that the observed S(152 eV)/Fe(703 eV) ratio corresponds to approximately one monolayer of sulfur. Since sulfur is a well known poison for FT synthesis, this result suggests that complete reduction of this catalyst in hydrogen would result in little or no FT synthesis activity. This prediction is in agreement with our reactivity studies where reduction of the catalyst at 543 K for a week with 35 sccm of H_2 or at 723 K with 20 sccm of H_2 for 15 hours resulted in a catalyst that was completely inactive for FT synthesis.

Transmission Electron Microscopy

Fig. 4 shows a typical image of the primary particles that make up the spherical agglomerates of the UCI catalyst. These particles are single crystals of a-Fe_2O_3 as confirmed by electron diffraction[7]. These single crystals have a characteristic contrast consistent with the presence of

voids within the single crystal matrix. The circular features exhibit a characteristic light/dark contrast with changes in focus which is typical of voids. These voids do not disrupt the crystal structure since the lattice fringes go through them. In subsequent discussions, we refer to this microstructure as the "swiss-cheese" morphology.

Sample microstructure after activation

A 2 hr CO activation of 1 g of catalyst with 20 sccm of CO at 543 K transformed the a-Fe_2O_3 into Fe_3O_4 plus small amounts of carbide. The presence of the carbide was deduced from electron diffraction and is consistent with the results from XRD and CHN analysis. We find that the carbide is always covered with a surface film which we attribute to amorphous carbon. Activation in the syngas mixture for 2 h at 523 K shows no carbide but only magnetite. In these images, the presence of magnetite is seen by electron diffraction as well as by the presence of regions with remnants of the "swiss-cheese" morphology of the original hematite catalyst. Activation in H_2 for 15 hours at 723 K of 1 g of catalyst transformed the sample to α-Fe as confirmed by XRD and electron diffraction. A thin film of oxide formed on the surface of the sample during the controlled passivation in the reactor. Electron diffraction showed a faint ring indicating the presence of polycrystalline magnetite. This oxide film was different in appearance from the magnetite resulting from the phase transformation of hematite which retained the "swiss-cheese" morphology. Furthermore, the crystallinity of the film helped to distinguish it from the amorphous and graphitic carbon that forms during exposure to syngas or to CO.

Sample microstructure after activation and 10 hour reaction

After a short reaction period, sample morphologies are quite different. The CO-activated sample shows a much greater degree of transformation into carbide, while the syngas activated sample shows a smaller extent of carbide formation. The carbide particles grow out of the magnetite as nodules on the surface (For example, Fig. 5). This phase transformation starts to break up the initial single crystal "swiss-cheese" morphology by outgrowth of the carbide phase. The carbide particles are invariably covered by a surface film while the magnetite surface is clean. We attribute these surface films to amorphous carbon formed during reaction.

Sample microstructure after activation and 45 hour reaction

After a 45 hour reaction, all samples show significant amounts of carbide formation, although the FT activated samples still have some magnetite present. The CO activated sample shows very small traces of magnetite. A common feature in all samples, irrespective of the nature of the activation treatments or the extent of the reaction, is the occurrence of 3-4 nm thick films of amorphous carbon *only* on the carbide particles. See Fig. 6. The magnetite phase, where present, is not covered by any overlayers. With electron and X - ray diffraction, it is not possible to distinguish between the various carbide phases since they all had primary diffraction peaks extremely close to each other. The major peak from the carbide formed in our samples is a broad reflection centered around a 2q value of 43°. In the TEM images, carbide grains appear as small crystallites showing d spacings of ~2Å. For this reason, we have chosen to label the carbide phase as a single iron carbide without reference to its precise stoichiometry.

The role of activation

When iron catalysts are exposed to FT synthesis reaction environments, the catalysts transform from hematite into one or more carbides, regardless of the activation step. The activation process controls the rate of the transformations. The single crystals of hematite first transform into magnetite retaining the characteristic "swiss cheese" morphology. This step is relatively facile and is complete within 2 hours at 543 K for all activation treatments. We have shown that this

transformation can occur at lower temperatures[7]. The subsequent transformation from magnetite to carbide is slow and depends on the activation environment. The carbide phase forms as small nodules on the surface of the magnetite with the phase transformation proceeding slowly into the bulk. The breakdown of the original single crystals is brought about by this phase transformation.

Based on the rate of CH_4 formation, which we consider to be an indication of FT activity, we find the CO activation to be the most effective method for activating the catalyst. Activation in CO transforms the hematite into magnetite and small amounts of carbide at the end of the 2 hour activation step. With CO/H_2 activation under mild conditions, we see only magnetite and the catalyst shows no initial FT activity, although some CO_2 is formed. When syngas activation was performed at 543 K, we did see evidence of initial FT activity and the presence of carbide. However, the subsequent activity as a function of time is very similar to that of the sample activated at 523 K.

These morphological transformations involve a major breakdown of the single crystal hematite particles into smaller crystallites of carbide, but there is no corresponding increase in the BET surface area, which remains at ~27 m^2/g (the surface area of the as-received catalyst). The hematite crystals are platelets about 1 μm long, 0.3 μm wide and approximately 40-50 nm thick. The surface area can be calculated as follows:

$$S = \frac{2LW + 2(L+W)d}{\rho LWd}$$

$$S \approx \frac{2}{\rho d}$$

when $d << L, W$

Based on these equations, a BET surface area of 27 m^2/g corresponds to a thickness of about 15 nm for particles of density 4.7 g/cm^3 (from helium pycnometry). However, the observed thickness of the crystallites is about 40-50 nm, which is greater than the calculated value. The discrepancy is probably due to the "swiss cheese" morphology of the single crystals which may serve to enhance the surface area beyond the value calculated from the geometry of the particles.
During reaction, the hematite breaks down into carbide crystallites that are 20-30 nm in diameter. The surface area of the catalyst after reaction (21-24 m^2/g) is not very different from the original surface area. This surface area is consistent with spherical particles of diameter 38-34 nm and density 7.4 g/cm^3 (carbide), in agreement with particle sizes observed by HRTEM. The BET surface area does not change significantly as the catalyst is activated and used for reaction. Since the BET surface area includes contributions from the oxide and carbide phases along with the possibility that the surface carbon overlayers are porous, the BET surface area does not serve as a good indicator of catalyst activity.

The nature of the active phase
Our results indicate that the magnetite is not catalytically active, but transformation of the magnetite into carbide is a prerequisite to obtain FT activity. This is seen in the lack of initial methane formation on the sample activated in syngas at 523 K which had only magnetite at the end of the activation step. The CO activated sample was the only one that contained some carbide, and it shows a significant methane formation rate immediately after introduction of the syngas mixture. On the syngas activated samples, the rate of methane formation is seen to increase commensurate with the slow increase in carbide formation as seen in the TEM images, by XRD, and from the amount of carbon in the sample as measured by bulk CHN analysis.

Based on the TEM and XRD results, we cannot specify the stoichiometry of the carbide phase that is formed on our catalyst. If the active phase was c-$Fe_{2.5}C$, we would expect to see approximately 7.9 wt% carbon in the sample. After a 10 hour reaction with the CO activated sample, we have 6.85 wt% C and the sample still contains some magnetite as seen by XRD and TEM. The peak activity for methanation is achieved at this point. Therefore, our data would be consistent with the c-$Fe_{2.5}C$ being the active phase in these catalysts. The CO-activated sample showed some deactivation after 45 hours which was accompanied by an increase in carbon content. This suggests that carbonaceous layers were deposited on the sample which slow down reaction, as seen in TEM images.

The initial low activity of the catalysts activated in syngas can be related to smaller extents of carbide formation. Even after 45 h on stream the syngas activated sample contains 5.1 wt% C, which suggests that the sample has still not completely transformed into the carbide. This observation is confirmed by TEM and XRD which show larger amounts of magnetite present on these samples than for the CO-activated sample. The amount of carbon seen by bulk elemental analysis and the extent of carbide formation seen by TEM and XRD was the lowest in the case of the isothermal syngas reaction at 523K. This suggests that the higher temperature 543K treatment is necessary to accelerate the solid state transformation from magnetite into carbide.

Our conclusion that the transformation of magnetite into carbide is necessary to obtain FT synthesis activity in iron catalysts is consistent with the competition model proposed by Niemantsverdriet et al.[89] This model states that the initial low activity of metallic iron is due to rapid diffusion of carbon atoms into the iron to form carbide, thereby removing carbon atoms from the surface and rendering them unavailable for FT reactions. As bulk carbiding approaches completion, the rate of diffusion of carbon decreases and the amount of carbon available on the surface for FT reactions increases. Within this model, the bulk carbide is not necessarily the active phase, but carbide formation must occur before the catalyst surface can retain enough carbon to become active. Similar arguments can explain the effects of the magnetite to carbide transformation on the FT activity of the catalyst studied in this work. The syngas-activated catalyst consists primarily of magnetite, which is inactive for FT. Upon exposure to the syngas mixture, first magnetite forms, then CO is consumed mainly by conversion of magnetite to carbide. Once carbide is formed, any additional CO dissociation results in the formation of active carbon on the carbide particle surfaces or deposition of inactive graphitic carbon overlayers. Consequently, FT activity increases with the extent of transformation of magnetite into carbide. For the CO activated catalyst, carbide formation has already occurred to some extent prior to introduction of syngas, and the surfaces of these precarbided particles are active for FT synthesis immediately upon introduction of the syngas mixture. Ultimately, the buildup of inactive, graphitic carbon on the carbide particle surfaces inhibits the FT reaction and activity begins to decrease, resulting in the observed maximum in FT activity. Based on the TEM and activity results and the proposed model, nothing can be said about the nature of the active sites on the surface of the carbide particles, except that the formation of bulk carbide is necessary before the active site can be formed.

After performing FT synthesis on an unreduced iron oxide catalyst, Kuivila, et al.[10] observed 22% carbide in the bulk by Mössbauer spectroscopy, but only ~3% carbide on the surface by XPS, and therefore concluded that a sub-surface carbide phase had formed beneath a magnetite surface layer. Based in part on this result, they conclude that magnetite is the active phase for FT synthesis. Reymond, et al[6] also observed substantial amounts of carbide by XRD, but little or no carbide by XPS. Our observation of a 3-4 nm thick carbon layer on the carbide phase, but not on the

magnetite, allows a reinterpretation of the data in these two papers that does not require the counterintuitive concept of carbide formation beneath an oxide layer. In the presence of this carbon layer, the Fe 2p photoelectrons from the carbide would be attenuated by a factor of exp(-d/l) = 0.07 to 0.13, where l = 1.5 nm is the attenuation length of Fe 2p photoelectrons and d = 3 to 4 nm is the carbon layer thickness. Since the magnetite signal is unattenuated (no carbon buildup occurs on the magnetite phase), a bulk composition of 22% carbide would result in an apparent surface composition of only ~2-4% carbide as measured by XPS, exactly as observed by Kuivila, et al[10] and consistent with our results and the qualitative results of Reymond, et al[6]. Thus, measurement of low carbide signals by XPS cannot be interpreted to mean that carbide is absent from the catalyst surface, and therefore not an important phase in FT synthesis. Indeed, the difficulties involved in using XPS to detect carbide in the presence of oxide means that for partially carbided iron catalysts, XPS is not likely to shed any light on the chemical state of iron at the surface of the carbide particles. For a fully carbided catalyst, however, where the entire Fe 2p signal arises from the carbide particle surfaces, XPS could still prove useful in elucidating the nature of the iron at the surface of the particles.

The conclusion of Kuivila, et al.[10] that magnetite and not carbide is catalytically active also contradicts their findings of lower, but not zero, FT activity of the metallic Fe catalyst. The metallic Fe catalyst has undoubtedly no magnetite to start with. In their experiments, the CO turnover frequency seems to correlate well with the extent of carbide formation in agreement with our observations that methanation activity follows the increase in carbide content.

High-pressure, Slurry-phase Iron Catalysts

All the above samples were taken from a 1 atm reaction, which may not represent the morphologies found at industrial conditions. In order to gain insight to the morphological changes of an iron catalyst under more realistic conditions we obtained samples of a Fe/4.4Si/O.71K catalyst from Prof. B. H. Davis, University of Kentucky that were subjected to FT synthesis in a slurry phase reactor for progressively increasing lengths of time. The reaction was carried out at 543 K and 175 psig with H_2/CO=0.7 and a total space velocity of 2.0 nL h^{-1} g^{-1} (Fe). The samples were extracted after varying lengths of time ranging from 6.33 h to 456 h. Although there was no initial activation treatment for the catalyst, after 93 h of FT reaction, H_2 flow was stopped and CO flow was increased to of 2.0 nL h^{-1} g^{-1} (Fe). This was done for 22 h after which the original conditions were restored. The conversion increased significantly after the intermediate CO flow. Two samples were studied by TEM. The first, #RJO-177A, was taken from the reactor after 6.33 h on stream. The second sample, #RJO-177G, was taken from the reactor after 192.5 h on stream, about 80 h after the CO activation. This second sample, #RJO-177G, showed an activity of about four times that of the first sample.

The TEM of RJO-177A shows crystallites having an average diameter of 10 nm. The particle surfaces are mostly clean, i.e., free of carbon overlayers, however high resolution views indicate an occasional particle surrounded by overlayers of graphitic carbon. The diffraction pattern corresponds to the magnetite phase although the spotty nature of the diffraction ring pattern indicates larger crystals of magnetite. If the carbide phase is present, it is not possible to conclusively establish its existence since the various iron carbide phases have d-spacings around 2A which overlap with the (400) plane of Fe_3O_4. The TEM of RJO-177G, Fig. 7, showed the presence of a large number of crystallites which are covered by surface overlayers. The diffraction pattern shows rings consistent with magnetite although it is diminished in intensity compared to the pattern found for RJO-177A.

Because of the amount of graphitic carbon found in close proximity to magnetite in RJO-177G, it is not clear whether this catalyst reacted at higher pressures contains a greater amount of magnetite than the samples reacted at 1 atm or whether there was a passivation problem with these catalysts. This will be pursued further.

Conclusions

We have studied the role of various phases that are formed when an iron oxide catalyst is activated for the Fischer-Tropsch synthesis reaction. Our study shows that during activation, the iron oxide transforms from hematite to magnetite and finally into an iron carbide phase. As the carbide content of the catalyst increases, we see the development of FT activity as measured by the rate of methane formation and CO consumption. Neither magnetite nor hematite were found to have any FT activity. Based on this correlation between carbide formation and activity, we conclude that carbide formation is necessary before iron FT catalysts can exhibit any activity. The exact nature of the surface phase on which the reaction takes place remains elusive, however, due to an inability of surface sensitive techniques such as XPS to penetrate an amorphous carbon film which forms on the carbide particles during FT synthesis. These amorphous carbon films may hinder diffusion of the reactants to the catalyst surface, leading to eventual deactivation of the catalyst after long periods of reaction, and providing an explanation for the observation that the catalyst activity first increases and then starts to fall while the carbide content is still increasing. The formation of the carbide phase activates the catalyst while the simultaneous build-up of carbon on the carbide leads to deactivation. The phase transformations in the catalyst play an important role in determining the activity, attrition resistance, and deactivation of this catalyst. Activation of this precipitated catalyst transforms single crystals of hematite to smaller crystallites of carbide. While the transformation from hematite to magnetite is extremely rapid, the magnetite to carbide transition is much slower under the conditions of temperature and pressure employed in our study. As carbon deposits on the carbide particles, it serves to further pry the carbide particles apart.

Comparison of the various activation treatments indicates that CO activation is able to transform the iron oxide catalyst most rapidly into the carbide phase, and thereby results in the most active catalyst. H_2 reduction to metallic iron may not necessarily be desirable since it causes the sulfur impurities to segregate to the catalyst surface. The slowest activation was seen in syngas at reaction temperature (523 K), suggesting that activation at 543 K may be necessary to obtain higher catalyst activities at short times.

---

[1] Sault, A. G., *J. Catal.*, **140**, 121 (1993)

[2] Joint Committee for Powder Diffraction Standards, pub: JCPDS, International Center for Diffraction Data.

[3] Kuivila, C.S., Butt, J. B. and Stair, P. C., *Appl. Surface Sci.*, **32**, 99 (1988).

[4] Sault, A. G. *Appl. Surface Sci.*, **74**, 249 (1994).

[5] Davis, L.E., McDonald, N. C., Palmberg, P. W. Riach, G. E., and Weber, R. E., "Handbook of Auger Electron Spectroscopy." Perkin-Elmer Corp., Eden Prairie, MN 1978.

[6] Reymond, J. P. , Meriaudeau, P. and Teichner, S. J., *J. Catal.*, **75**, 39 (1982).

[7] Shroff, M. D., Kalakkad, D. S., Coulter, K.E., Kohler, M.S., Harrington, Jackson, N. B., Sault, A. G., and Datye, A. K., *J. Catal., in press.*

[8] Niemantsverdriet, J. W., van der Kraan, A. M., van Kijk, W. L., and van der Baan, H. S., *J. Phys. Chem*, **84**, 3363 (1980).

[9] Niemantsverdriet, J. W., van der Kraan, A. M., *J. Catal.*, **72**, 385 (1981).

[10] Kuivila, C. S., Stair, P. C., and Butt, J. B., *J. Catal.*, **118**, 299 (1989).

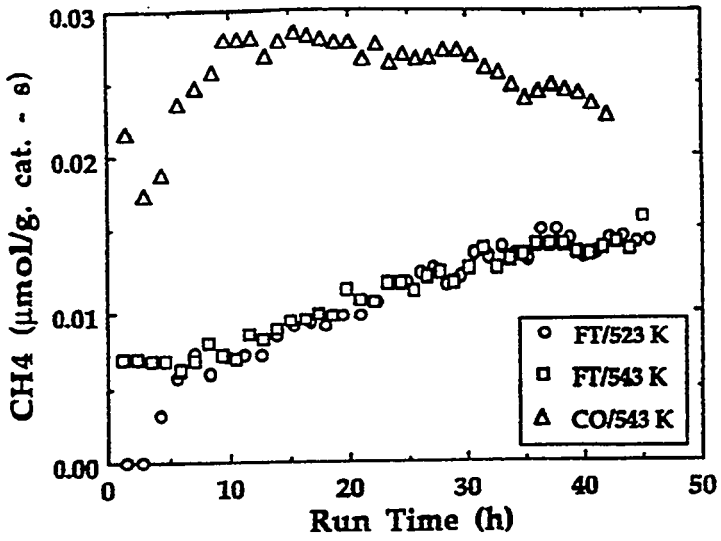

Figure 1. CH_4 formation during FT synthesis over time with various activation treatments.

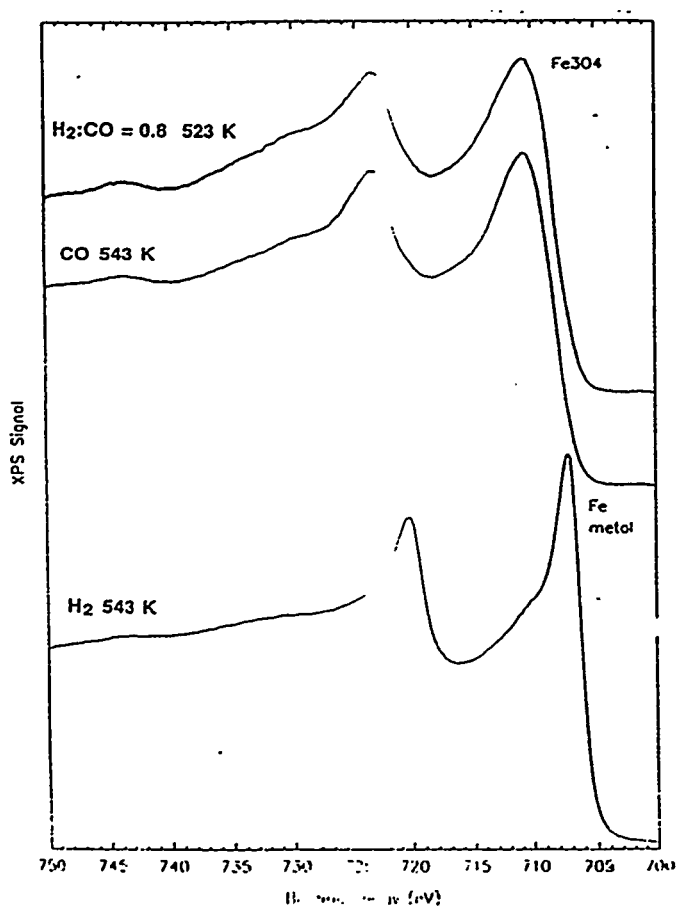

Figure 2. XPS of iron catalyst following three different activations.

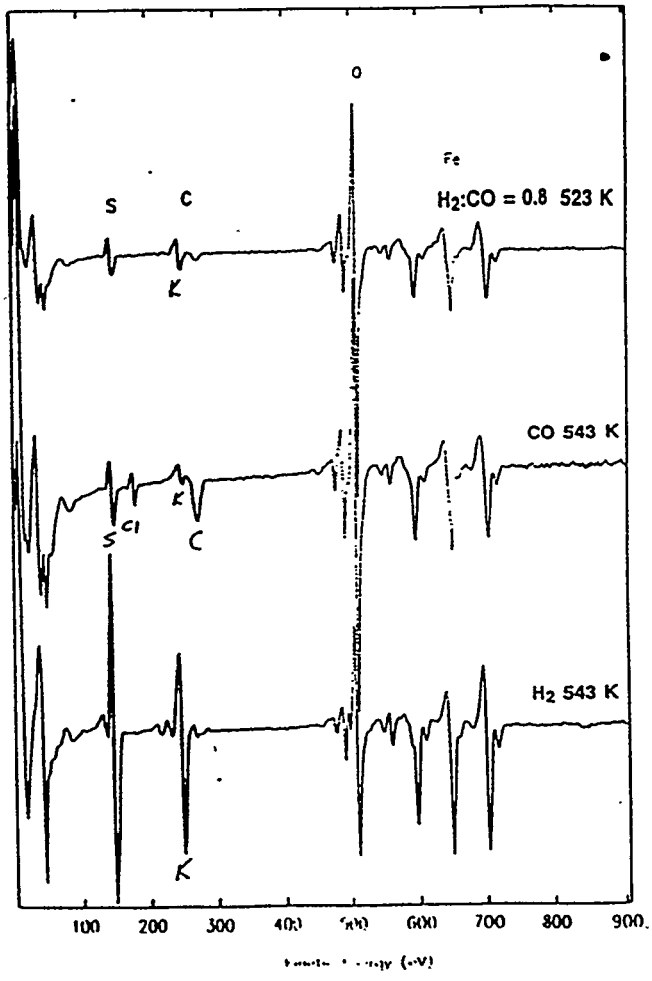

Figure 3. Auger spectra taken after three different activations.

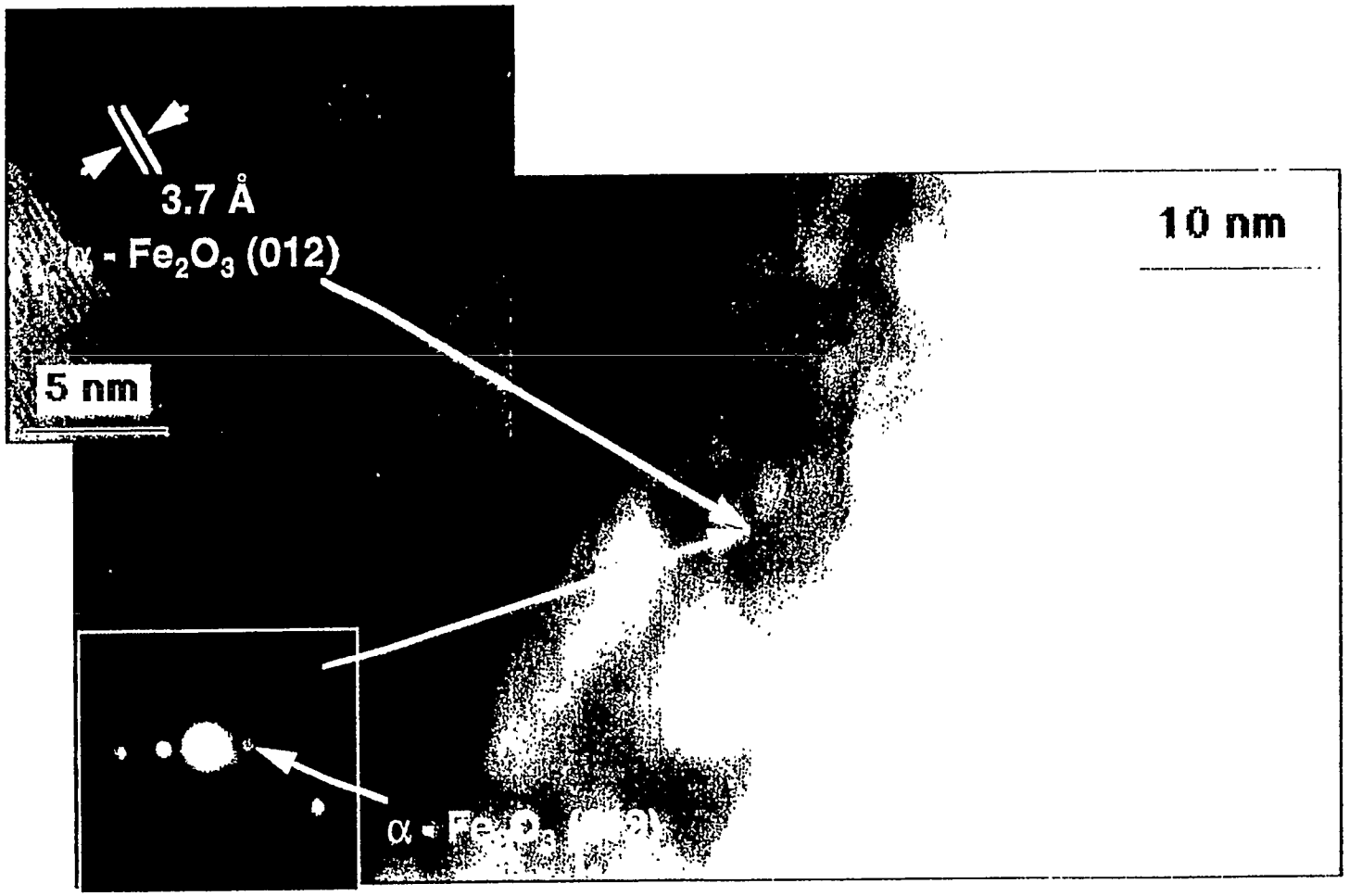
3.7 Å
α - Fe2O3 (012)
5 nm
10 nm

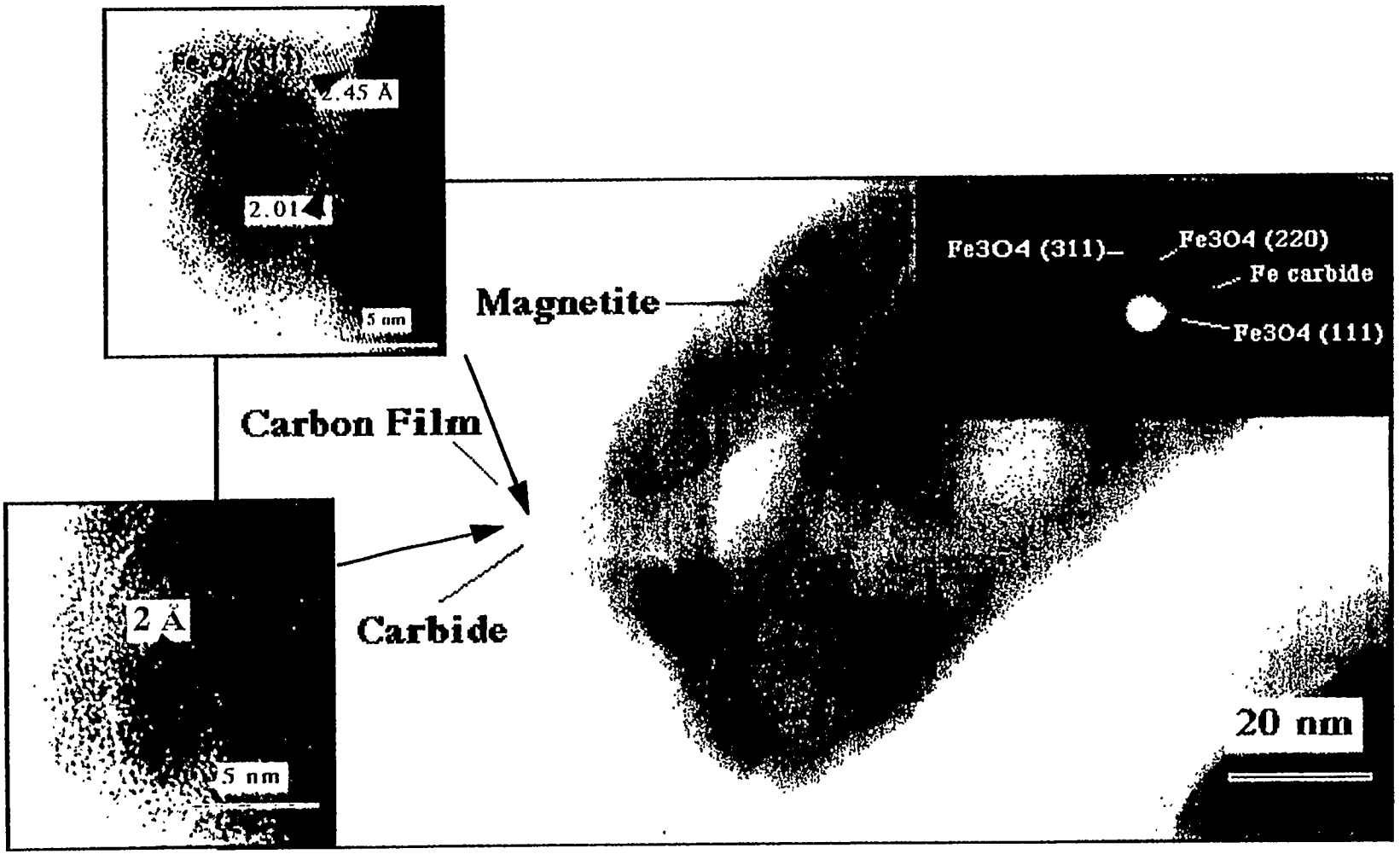
2.45 Å
2.01
5 nm
Magnetite
Carbon Film
Carbide
2 Å
5 nm
Fe3O4 (311)
Fe3O4 (220)
Fe carbide
Fe3O4 (111)
20 nm

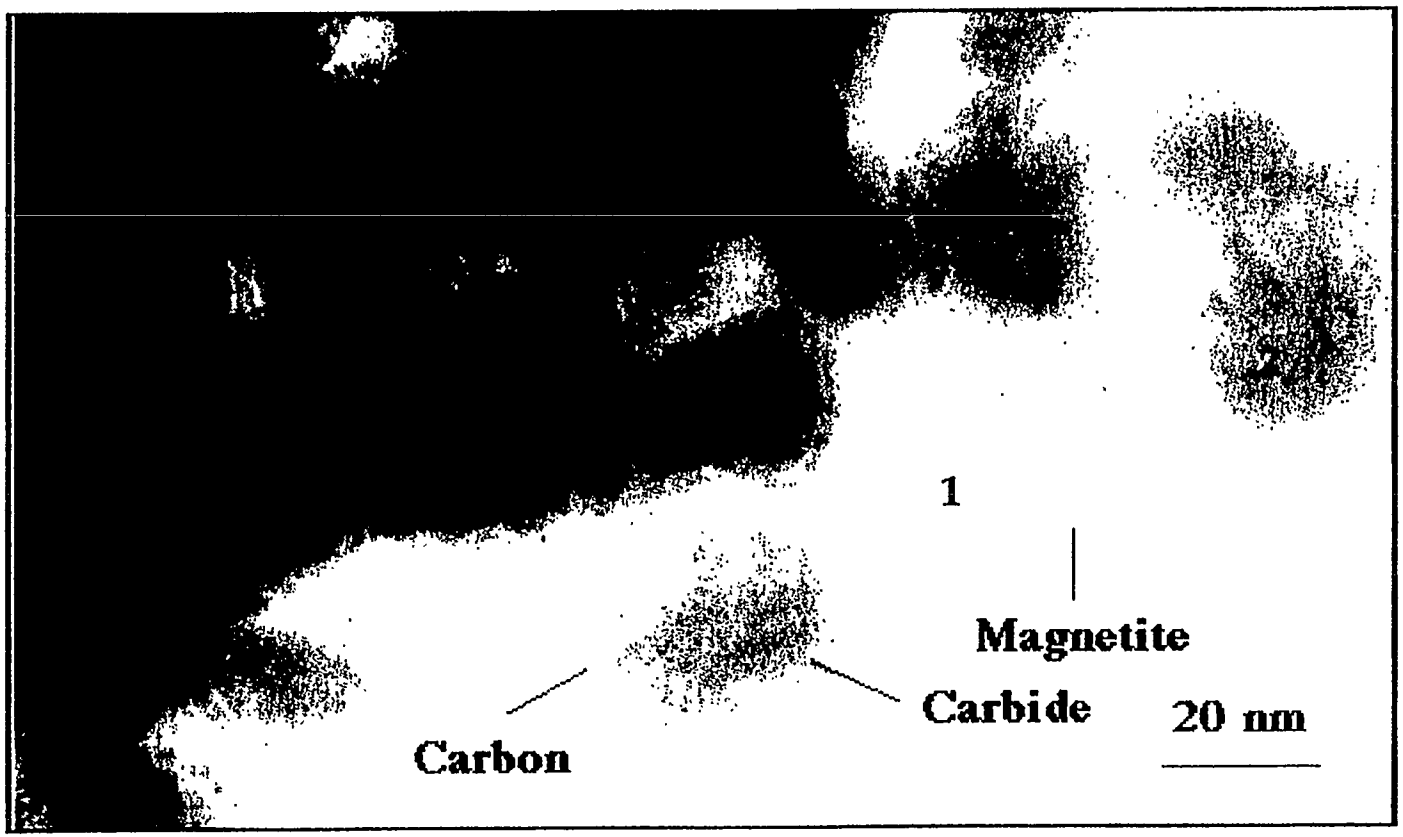
1
Magnetite
Carbide
Carbon
20 nm

Fig. 7

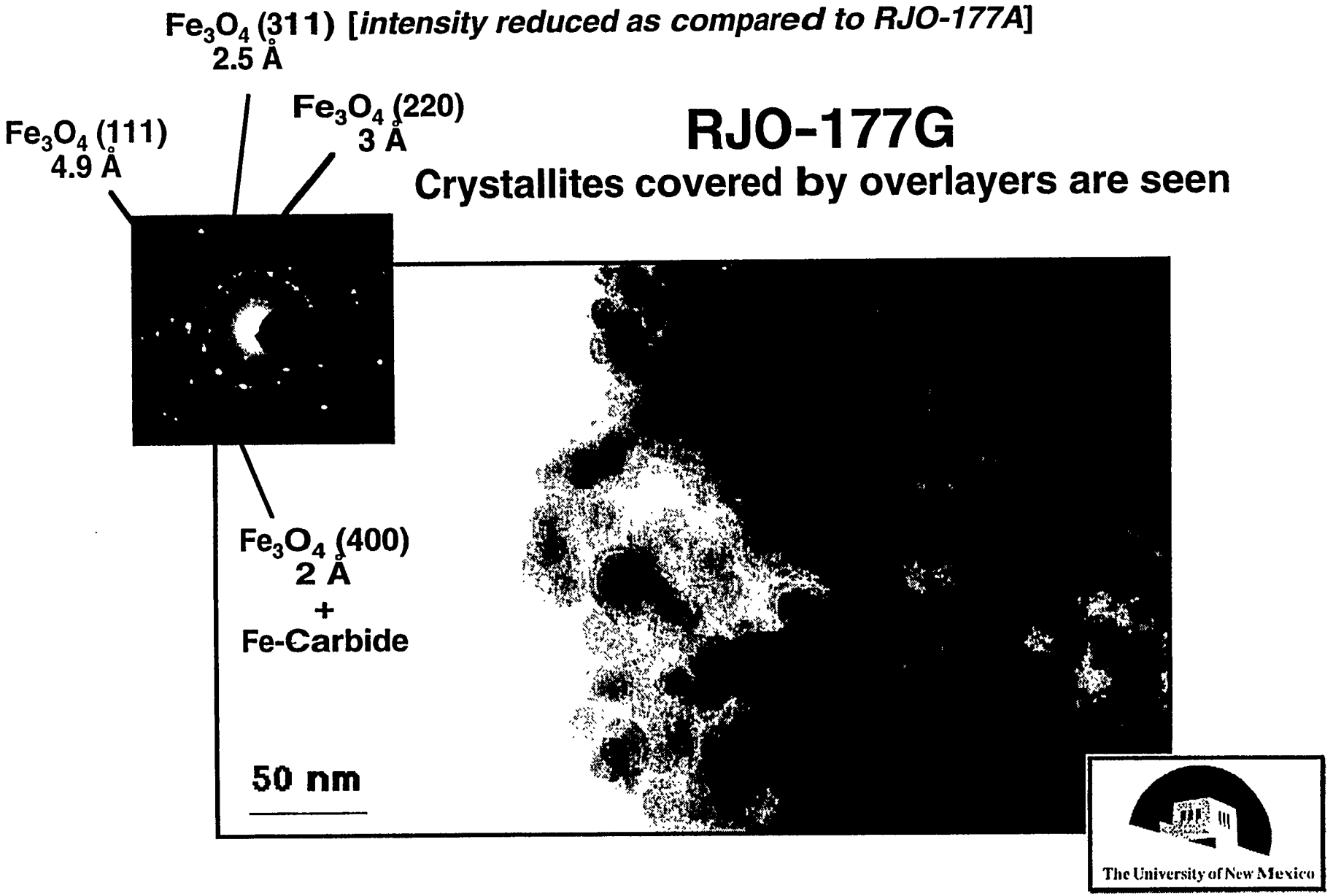
Fe_3O_4 (311) [*intensity reduced as compared to RJO-177A*]
2.5 Å
Fe_3O_4 (111)
4.9 Å
Fe_3O_4 (220)
3 Å
RJO-177G
Crystallites covered by overlayers are seen
Fe_3O_4 (400)
2 Å
+
Fe-Carbide
50 nm
The University of New Mexico